

14B.6

Retrieval of Moisture from GPS Slant-path Water Vapor Observations using 3DVAR with Isotropic and Anisotropic Recursive Filters

Haixia Liu^{1,2}, Ming Xue^{1,2}, R. James Purser³ and David F. Parrish⁴

¹Center for Analysis and Prediction of Storms and ²School of Meteorology
University of Oklahoma, Norman OK 73019

³Science Applications International Corporation, Beltsville, Maryland

⁴Environmental Modeling Center, National Centers for Environmental Prediction
Camp Springs, MD 20746-4304

1. Introduction

It is the lack of the knowledge of fine-scale spatial and temporal variations of water vapor that partly results in the slow improvement in quantitative precipitation forecast (QPF). The International H₂O Project (IHOP, 13 May through 25 June 2002; (Weckwerth et al. 2004)), consequently, was conducted in summer, 2002 to investigate the four-dimensional distribution of atmospheric water vapor and its impact on QPF. During IHOP, a network of sensors collected numerous water vapor data. This network included ground-based GPS receivers which measure the delay along the slant path from GPS satellites to the ground-based receivers. The water vapor information can be derived from the slant-path wet delay (the part of the delay caused by the water vapor) (Rocken *et al.* 1993; Ware *et al.* 1997; Braun *et al.* 2001).

Due to the integrated nature of the GPS observations, variational method is the natural choice for analyzing such data. Most of the earlier work utilizing variational methods examined the impact of the vertically integrated water vapor, or precipitable water (*PW*), or the zenith total delay (*ZTD*) data (Kuo et al. 1993; Kuo et al. 1996; Guo et al. 2000; De Pondecia and Zou 2001a; De Pondecia and Zou 2001b; Falvey and Beavan 2002; Cucurull et al. 2004). Despite the fact that they all found a positive impact of assimilating the GPS data on precipitation forecast, there is a loss of information content when using derived *ZTD* or *PW* data as compared to the original slant-path data, due to the spatial and temporal averaging involved in their derivation. It should, therefore, be beneficial to exploit the slant-path total or wet delay or slant-path water vapor (*SWV*) data directly. The multiple slant paths form, in a sense, a 'net', that provides a much better three-dimensional (3D) coverage than the vertical-only zenith paths. Further discussions on the GPS data in various forms can be found in Liu and Xue (2005). So far, there has been only a very limited number of studies that directly analyze slant-path data (MacDonald et al. 2002; Ha et al. 2003; Liu and Xue 2005), all utilizing simulated

data from hypothetical GPS networks. These works demonstrated the effectiveness of slant-path data in recovering 3D moisture information.

To date, most variational analysis systems use static background error statistics that are flow independent. For slant-path GPS data, MacDonald et al. (2002) did not use a model background term. Ha et al. (2003) assumed the background error covariance is diagonal in their four-dimensional variational (4DVAR) system. It is, however, well known that flow-dependent background error covariance plays an important role in data assimilation. Such error covariance is usually spatially inhomogeneous and anisotropic. The background error covariance builds the relationship between the grid points and determines how the observation innovations are spread in the analysis domain. The reliable estimation of the degrees and orientations of anisotropy in the moisture background errors is likely more important for moisture analysis and QPF forecast because of the high spatial variability in moisture.

In our recent study (Liu and Xue 2005), a 3D variational (3DVAR) analysis system is developed that models the flow-dependent background error field using an explicit spatial filter. Better moisture analysis from simulated GPS slant-path water vapor data is obtained when using an anisotropic spatial filter based on the flow-dependent background error. The explicit filter, when applied over even a moderate number of grid points in three dimensions, is still expensive in terms of both computational and memory storage costs. A much more computationally efficient algorithm is the implicit recursive filter, whose flow-dependent anisotropic version, through much more complex than the isotropic version, has seen significant development very recently (Purser et al. 2003a, b). In this paper, we implement the recursive filter with an anisotropic opinion in our 3DVAR analysis system. We perform retrieval experiments of GPS slant-path water vapor data and compare the results with those of explicit filters.

The rest of this paper is organized as follows. Section 2 describes our 3DVAR system and a scheme for determining flow-dependent background error

covariances. It also describes the procedure for determining the recursive filter coefficients, especially for the anisotropic case, given the modeled covariances. Section 3 introduces our hypothetical ground-based GPS observation network and the simulation of GPS slant-path data. After illustrating in section 4 the effect of recursive filter on analysis with a single observation tests, we apply in section 5 our 3DVAR system to the 3D moisture retrieval. In section 6, we check the effect of filter length scales on the analysis quality and the sensitivity of the analysis to observational errors. Conclusions are given in section 7, together with a future plan.

2. 3DVAR system with recursive filters

We present in this section the 3DVAR analysis developed and used in this study. It is based on the 3DVAR system developed by LX05 hereafter. It uses a preconditioner that involves the square root of the background error matrix, \mathbf{B} , instead of \mathbf{B} itself as in LX05. As a result, the control variables of the incremental 3DVAR are different from those used in LX05. Further, it uses a recursive filter instead of an explicit spatial filter to model the effect of \mathbf{B} . The details are given below.

a. 3DVAR cost function

A variational method is to find an analysis that minimizes a predefined cost function. In this study, the cost function is defined as,

$$J(\mathbf{x}) = J_b(\mathbf{x}) + J_{swv}(\mathbf{x}) + J_{sfc}(\mathbf{x}) + J_c(\mathbf{x}), \quad (1)$$

where,

$$J_b(\mathbf{x}) = \frac{1}{2}(\mathbf{x} - \mathbf{x}_b)^T \mathbf{B}^{-1}(\mathbf{x} - \mathbf{x}_b), \quad (2a)$$

$$J_{swv}(\mathbf{x}) = \frac{1}{2}[H_{swv}(\mathbf{x}) - \mathbf{SWV}]^T \mathbf{R}_{swv}^{-1}[H_{swv}(\mathbf{x}) - \mathbf{SWV}], \quad (2b)$$

$$J_{sfc}(\mathbf{x}) = \frac{1}{2}[H_{sfc}(\mathbf{x}) - \mathbf{q}_{v_{sfc}}]^T \mathbf{R}_{sfc}^{-1}[H_{sfc}(\mathbf{x}) - \mathbf{q}_{v_{sfc}}], \quad (2c)$$

$$J_c(\mathbf{x}) = \frac{1}{2}(\mathbf{x} - |\mathbf{x}|)^T \mathbf{W}_c(\mathbf{x} - |\mathbf{x}|). \quad (2d)$$

The cost function J is composed of four terms. The first is the background term and the second and third are, respectively, the observational terms for GPS SWV and regularly surface moisture observations. The physical requirement that water vapor is not negative is expressed in the last term as a non-negative weak constraint. Superscripts '-1' and 'T' denote inverse and transpose, respectively. For clarity, the notations in the Eq. (2) are listed as follows.

\mathbf{x} : analysis variable or control variable vector. It is in our case the 3D specific humidity field.

\mathbf{x}_b : analysis background or first guess.

$\mathbf{q}_{v_{sfc}}$: surface observation vector of specific humidity.

\mathbf{B} : background error covariance matrix. This study focuses on the effect of \mathbf{B} in isotropic and

anisotropic forms on the analysis. Assuming the background error variances are homogeneous, i.e., equal to a constant in the analysis domain, then \mathbf{B} is the product of this constant (the reciprocal of the background error variance) and background error correlation coefficients.

\mathbf{SWV} : a vector containing the GPS slant path water vapor observations.

H_{swv} : forward observation operator which calculates GPS integrated SWV observations between GPS satellites to ground-based receivers from water vapor values at grid points.

H_{sfc} : forward observation operator for conventional observations of surface specific humidity.

\mathbf{R}_{swv} and \mathbf{R}_{sfc} : observation error covariances for SWV and surface moisture observations respectively. The observation errors are assumed to be uncorrelated therefore the error covariances are diagonal. Usually, the diagonal elements of \mathbf{R}_{swv} (\mathbf{R}_{sfc}) are the SWV (surface moisture) observation error variances. Assuming the error variances are independent of stations, then \mathbf{R}_{swv} and \mathbf{R}_{sfc} can be simplified as a constant (the reciprocal of the observation error variances) multiplying an identity matrix.

W_c : the weight (scalar) for non-negative weak constraint. It is specified to be 50 in our experiments.

Another point to be clarified is that in this study the reciprocals of error variances are specified in terms of the weights for observations and background terms. The relative weights of 1, 100 and 500 are given to the background, SWV and surface moisture observational terms, respectively. Much higher weights given to the observation terms reflect the high accuracy of observations compared to the background. Except for one experiment, the simulated data are assumed error free, i.e., no errors are added to the simulated observations. This is because we are most interested in investigating how well our recursive-filter-based 3DVAR scheme is able to recover the 3D specific humidity field under an ideal setting. Similar is done in LX05. We will also compare our results with those of similarly configured experiments using explicit spatial filters reported in LX05.

Usually, the dimensionality of matrix \mathbf{B} is too large to directly compute or store in entirety. To avoid the inversion of \mathbf{B} and to improve the conditioning of the minimization problem, a new control variable, \mathbf{v} , is defined which satisfies

$$\delta \mathbf{x} = \sqrt{\mathbf{B}} \mathbf{v}, \quad (3)$$

where $\delta \mathbf{x} \equiv \mathbf{x} - \mathbf{x}_b$ is the increment of \mathbf{x} .

The cost function can then be rewritten as,

$$\begin{aligned}
 J(\mathbf{v}) = & \frac{1}{2} \mathbf{v}^T \mathbf{v} + \frac{1}{2} \left[H_{\text{snv}}(\mathbf{x}_b + \sqrt{\mathbf{B}}\mathbf{v}) - \mathbf{S}\mathbf{W}\mathbf{V} \right]^T \mathbf{R}_{\text{snv}}^{-1} \left[H_{\text{snv}}(\mathbf{x}_b + \sqrt{\mathbf{B}}\mathbf{v}) - \mathbf{S}\mathbf{W}\mathbf{V} \right] \\
 & + \frac{1}{2} \left[H_{\text{yfc}}(\mathbf{x}_b + \sqrt{\mathbf{B}}\mathbf{v}) - \mathbf{q}_{\text{yfc}} \right]^T \mathbf{R}_{\text{yfc}}^{-1} \left[H_{\text{yfc}}(\mathbf{x}_b + \sqrt{\mathbf{B}}\mathbf{v}) - \mathbf{q}_{\text{yfc}} \right] \\
 & + \frac{1}{4} \left[\mathbf{x}_b + \sqrt{\mathbf{B}}\mathbf{v} - \left| \mathbf{x}_b + \sqrt{\mathbf{B}}\mathbf{v} \right| \right]^T \mathbf{W}_c \left[\mathbf{x}_b + \sqrt{\mathbf{B}}\mathbf{v} - \left| \mathbf{x}_b + \sqrt{\mathbf{B}}\mathbf{v} \right| \right].
 \end{aligned} \tag{4}$$

This new cost function contains no inverse of \mathbf{B} and the conditioning of the cost function is improved when the background error covariances play a key role.

The part of the role of background error correlation is to build the relationship between grid points such that the values at the grid points away from a station can be influenced by the observation innovation at that station. The effect of this correlation can be modeled using a spatial filter (Huang 2000) as follows,

$$b_{ij} = \exp \left[-\frac{1}{2} \left(\frac{r_{ij}}{L_r} \right)^2 \right], \tag{5}$$

where r_{ij} is the distance between two grid points i and j , L_r is the decorrelation length scale in terms of the grid intervals and is often linked to the observation density. This definition provides an isotropic background error covariance because the correlation only depends on the distance not direction. If L_r is constant, then the covariance is also spatially homogeneous. An alternative is the following anisotropic correlation,

$$b_{ij} = \exp \left[-\frac{1}{2} \left(\frac{r_{ij}}{L_r} \right)^2 \right] \exp \left[-\frac{1}{2} \left(\frac{f_i - f_j}{L_f} \right)^2 \right], \tag{6}$$

where f is a field whose pattern represents that of the background error. In this study, f is chosen to be either the true error field of the background or its estimate. The background field itself usually should not be used as f because the background and its error usually have different patterns. To estimate the f field, one possible way is to take advantage of the analysis increment, which will be discussed in detail in section 2c and section 5c. L_f is the decorrelation scale in the error field space in unit of k kg^{-1} for our moisture retrieval experiments. It controls the degree of the anisotropy.

b. Recursive filter

Compared to the explicit filter used in LX05, the recursive filter is much more cost effective. It is therefore implemented and tested in this study, for the purpose of modeling background error covariances. Purser *et al.* (2003a; 2003b) describe the construction and application of numerical recursive filters for the task of convolving a background error covariance. The two parts deal with spatially homogeneous and isotropic, and spatially inhomogeneous and anisotropic filters, respectively.

1) One dimensional recursive filter

The 3D filters can be created by the applications of multiple one-dimensional filters. The general n^{th} -order one-dimensional recursive filter has two steps (Hayden and Purser 1995). First the advancing step:

$$q_i = \beta p_i + \sum_{j=1}^n \alpha_j q_{i-j} \quad \text{for } i=1, \dots, N, \tag{7}$$

where p is the input and q is the output of the advancing step and n is the order of the recursive filter. The advancing step is followed by the backing step:

$$s_i = \beta q_i + \sum_{j=1}^n \alpha_j s_{i+j} \quad \text{for } i=N, \dots, 1 \tag{8}$$

where s is the final output from the recursive filter. Parameter α is the filter coefficient and have the relationship with β :

$$\beta = 1 - \sum_{j=1}^n \alpha_j. \tag{9}$$

2) Aspect tensor

For 3D problems, in the isotropic case, one simply applies three one-dimensional filters, one in each coordinate direction. In the anisotropic case, however, the background error covariance structure is constructed by applying six recursive filters, acting along six oblique directions. The filtering directions and the corresponding smoothing scales are determined by the aspect tensor defined at each grid point (Purser *et al.* 2003b). The aspect tensor \mathbf{A} is defined as follows for a Gaussian form,

$$\exp \left(-\frac{1}{2} \mathbf{x}^T \mathbf{A}^{-1} \mathbf{x} \right). \tag{10}$$

In order to find the aspect tensor at each grid point for the flow-dependent background error covariance defined in Eq. (6), it is necessary to rewrite Eq. (6) in a matrix form and a differential version. The finite difference $f_i - f_j$ is approximated by infinitesimal differential $d\mathbf{f}$ and distance r_{ij} is replaced by the differential $d\mathbf{x}$, then we obtain

$$\mathbf{B} = \exp \left(-\frac{1}{2} \left(\frac{d\mathbf{x}^T d\mathbf{x}}{L_r^2} + \frac{d\mathbf{f}^T d\mathbf{f}}{L_f^2} \right) \right), \tag{11}$$

where as before superscript T denotes transpose. This spatial reach of the anisotropic background error correlation should shrink along the direction of strong gradient of the error field compared to the corresponding isotropic one. For example, if the gradient of the error field is large in a given direction, then the difference in the background errors is large, i.e., df is large, so the background error correlation is small according to Eq. (11). Similarly, Eq. (10) is rewritten in a differential version as,

$$\exp\left(-\frac{1}{2}d\mathbf{x}^T\mathbf{A}^{-1}d\mathbf{x}\right). \quad (12)$$

Let Eq. (11) equal Eq. (12), then it comes out,

$$-\frac{1}{2}d\mathbf{x}^T\mathbf{A}^{-1}d\mathbf{x} = -\frac{1}{2}\left(\frac{d\mathbf{x}^T d\mathbf{x}}{L_r^2} + \frac{d\mathbf{f}^T d\mathbf{f}}{L_f^2}\right). \quad (13)$$

Differentiating above equation twice with respect to $d\mathbf{x}$ gives the inverse of \mathbf{A} as follows,

$$\mathbf{A}^{-1} = \frac{\mathbf{I}}{L_r^2} + \frac{\nabla\mathbf{f}^T\nabla\mathbf{f}}{L_f^2}, \quad (14)$$

where \mathbf{I} is the identity matrix and $\nabla\mathbf{f}$ is the gradient of f field. Here \mathbf{A} is symmetric and positive definite. The aspect tensors are locally defined at each grid point. For 3D problems, there are six filtering directions and the associated smoothing scales in these directions through each grid point. In fact, this leads to numerous one dimensional filters with varying scale lengths and directions. When L_f goes to infinity, the anisotropic filter reduces to an isotropic one. In this situation, the second term on the right hand side of Eq. (14) vanishes, so matrix \mathbf{A} reduces to the diagonal matrix which means the aspect tensor only includes three diagonal independent components and the filtering is only applied along the three coordinate directions and the filtering scale does not change with grid points when it depends only on the distance.

3) Hexad algorithm

The aspect tensor at each grid point can be derived from our flow-dependent background error covariances described above. Now the question is how to find the valid filtering directions and corresponding smoothing scales given an aspect tensor. Purser *et al.* (2003a) provide a what is called the ‘hexad algorithm’. The aspect tensor defined at each grid point can be represented as a positive combination of the components of a ‘canonical hexad’, with coefficients interpreted as the ‘spread’ component in the associated generalized direction. A detailed description of this algorithm can be found in the paper. In brevity, for a given aspect tensor, the hexad and weights (smoothing scales) are defined iteratively. A valid guess for hexad (filtering directions) must be provided, and then the corresponding weights can be computed from the known aspect tensor and the hexad. If the hexad is valid, these weights should all be non-negative and the task is completed. However, if some weights are negative, then the hexad is invalid and an alternative valid hexad must be sought. The algorithm eventually gives the uniquely valid hexad and the corresponding weights.

c. Estimation of background error field for anisotropic analysis

The variable f in Eq. (6) represents the background error field. For simulated observations, we know the ‘truth’ so the true background error is also known. We can consider the ‘true’ background error as f to obtain the aspect tensor \mathbf{A} for flow-dependent background error covariance according to Eq. (14). Then valid filtering directions and associated weights can be determined by the aspect tensor at each grid point. This is what will be done in ANISO experiment to be described in section 5b. But for realistic applications, the ‘true’ background error is not known in hand. In such a case, an estimate of the error is needed before we can perform any anisotropic analysis. Following LX05, we perform first an analysis using isotropic background error (as in experiment ISO), the difference between this analysis from the background is then used as an estimate of the background error field, i.e., as f in Eq. (6). An anisotropic analysis is then performed and this experiment is referred to as experiment UB, implying ‘Updated background error covariance \mathbf{B} ’. Such a two-step iterative procedure is in practice feasible, and is in a sense a double-loop strategy that is usually employed by operational systems of variational analysis (e.g., Courtier *et al.* 1994).

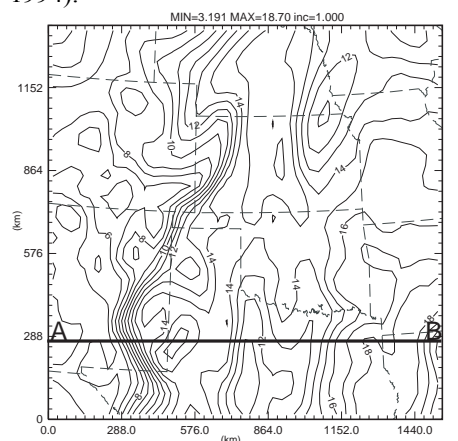


Fig. 1. Specific humidity field q_v (g kg^{-1}) of ‘nature’ run at the surface from ARPS simulation for an IHOP case valid at 20 UTC, 19 June, 2002. The analysis domain is 1620 km x 1440 km in Great Plain. The dryline is represented by the strong gradient of q_v . The thick line A-B is at $y = 270$ km.

3. Generation of simulated observations

As in LX05, simulated data will be used to test our analysis system in this study. With simulated data, both the truth and the error properties of the observations are known. With simulated data, future

observational networks can be tested. The Advanced Regional Prediction System (Xue et al. 2000; 2001; 2003) in a generalized terrain-following coordinate is used to simulate the 3D water vapor field of a dryline case occurring at 20 UTC, June 19, 2002, during the 2002 IHOP field experiment (Weckwerth et al. 2004). The generation of simulated observations is the same as in LX05. The true simulation is based on the configurations of CAPS (Center for Analysis and Prediction of Storms) real time forecast for IHOP (Xue et al. 2002). The analysis grid has a 36 km horizontal resolution, and the domain covers an area of 1620x1440 km² over the central Great Plains of U.S. The dryline is characterized by the strong moisture gradient. Its simulation result is considered as the ‘natural’ run or ‘truth’ of the atmospheric water vapor field shown in Fig. 1.

The formula as follows is utilized to produce the GPS slant-path water vapor observations.

$$SWV_{ij} = \int_{i^{th} \text{ receiver}}^{j^{th} \text{ satellite}} q_v ds, \quad (15)$$

where SWV_{ij} is the integrated water vapor along the slant path between the i^{th} ground-based receiver and the j^{th} GPS satellite, and q_v is the specific humidity along the path, based on the ‘truth’. The GPS observation network composes of 9 irregularly distributed satellites and 132 ground-based receivers which are evenly distributed in the analysis domain. There is one receiver station every four grid points, giving a receiver network resolution of 144 km in each horizontal direction.

4. Single observation tests

To assess the performance of the afore-described variational method using recursive filters and more importantly to understand the behaviors of the isotropic and anisotropic recursive filters, two single-observation experiments are performed using two-dimensional isotropic and anisotropic recursive filters, respectively. In such experiments, the SWV observation term is excluded from the cost function. Only one surface moisture observation located at grid point (12, 11, 1) in terms of the grid point index (marked by a filled black dot in Fig. 2), with a value of 14.72 g kg⁻¹, is analyzed. The background is set to a constant value of zero and the filter scales L_r is specified as 4

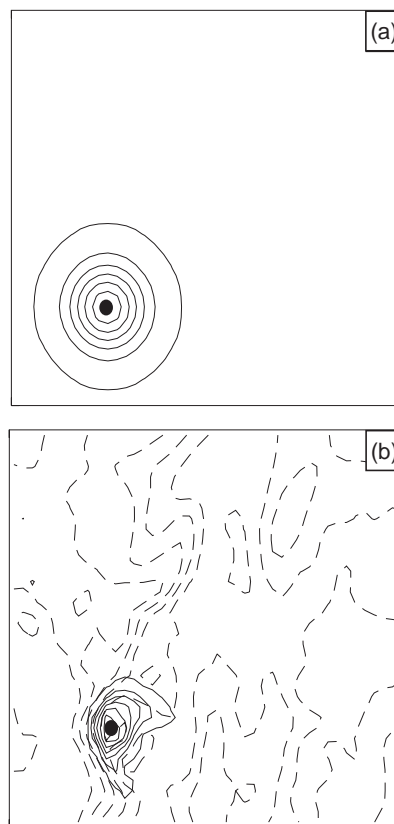


Fig. 2. Analysis from single observation experiments. (a) for the isotropic example whose analysis is of circular shape. (b) for anisotropic example coupled to a reference field (dashed lines). Strong anisotropy is illustrated. The correlation is stretched along the contours of the reference field.

grid intervals. Since the filters are two dimensional, there is no coupling among the vertical levels therefore the analyses are essentially two dimensional. We will therefore only examine the surface field, which is impacted by the single surface observation. Because the fourth-order recursive filter with one pass is accurate enough to reproduce the effect of the explicit Gaussian filter (Purser et al. 2003b), in these two experiments, fourth-order filtering is applied in each filtering direction. Fig. 2 shows the analyses from these two experiments. Since the background is zero, the analyzed fields are the analysis increments and should represent the corresponding structures of the background error covariance. Fig. 2a shows, as expected, the circular shape of the isotropic analysis increment. For the anisotropic case, L_r is also equal to 4 grid intervals, but L_f is specified as 2 g kg⁻¹. The ‘true’ moisture field shown in Fig. 1 is used as the reference field (error field f), for the analysis (because the background is zero). Strong anisotropy in the analysis increment is clearly revealed by Fig. 2b. The

correlation is stretched along the directions of contours of the reference field. The correlation decreases rapidly through the region where the reference field has a strong gradient, e.g., west of the single observation; in contrast, it decreases much more slowly northeast of the observation, where gradient is small. In the current ideal case where the background error covariance is modeled after the known truth, using an anisotropic recursive filter, the analysis should match the truth very well when a sufficient number of observations are present. This will be examined in the next section.

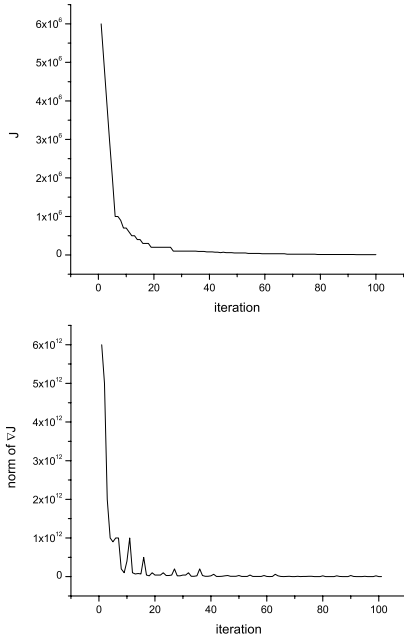


Fig. 3. The variation of the cost function J and the norm of the gradient ∇J with the number of iterations during the minimization procedure for experiment ISO.

5. Three-dimensional moisture analysis

The earlier single-observation experiments demonstrate that our analysis system with recursive filter performs as expected. Subsequently, we move to the analysis of full 3D water vapor field from simulated GPS *SWV* and surface moisture observations. Three experiments are conducted and discussed in this section, and they use three different forms of background error covariances. In the first experiment, called ISO, the correlation between any two points is only a function of their distance, so the covariance is isotropic; it is modeled using the isotropic recursive filter. The covariance is also assumed to be spatially homogeneous. For the latter two experiments, the correlation is the function of not only the distance but also the moisture state; the covariance is state-dependent (or flow-dependent) and is modeled using an anisotropic recursive filter.

For the first of the two, called ANISO, the error field is based on the truth field, i.e., the f field in Eq. (6) is equal to the ‘truth’ minus analysis background. Through this experiment we can determine how well our analysis system can recover the 3D humidity field from the *SWV* and surface moisture observations, under an ideal condition. For the second of the two anisotropic experiments (called UB), the iterative procedure described in section 2c is employed, in which an estimate of the error field, as the difference between the first isotropic analysis and the background is used as the error field, f , for the subsequent anisotropic analysis. In all three cases, the observational data are error free, and the analysis background was created by smoothing the ‘truth’ 50 times, using a 2-D 9-point filter in the horizontal.

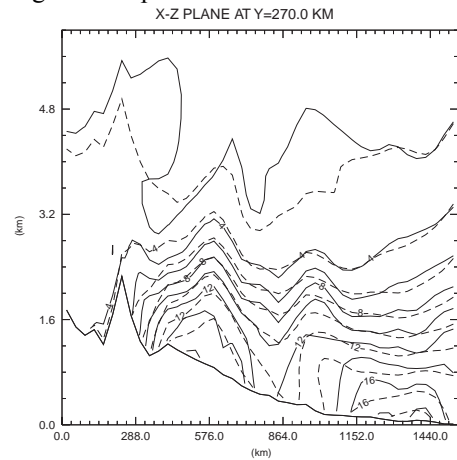


Fig. 4. East-west vertical cross-section of the retrieved specific humidity field (dashed lines) from experiment ISO at $y = 270$ km versus the ‘nature’ run (solid lines) in unit g kg^{-1} . Contour interval is 2 g kg^{-1} .

a. Analysis with an isotropic background error correlation model

The first experiment, ISO, uses an isotropic background error covariance. The fourth-order one-dimensional isotropic recursive filter is applied along each coordinate direction using one pass only (Purser *et al.* 2003b). The horizontal and vertical filtering scales are chosen to be five grid intervals. The choices of filtering scales are linked to the observation density. We want the observation innovation can be spread far enough to cover the gap between receiver stations. The weights of the background term, GPS *SWV* observations, the surface moisture observations and the non-negative weak constraint are specified as 1, 100, 500 and 50, respectively. The determination of their weights should depend on the reliability of each term and their relative importance in the analysis. Because we assume that the observations are error-free here, the observation terms are given much higher weights that

the background term. In another word, we do not trust the background. As a result, the final analysis should be much closer to the observations than to the background. The minimization algorithm used is the LBFGS method.

Figure 3 shows the cost function and the norm of the cost-function gradient as functions of the number of iterations during the minimization procedure for experiment ISO. The significant reductions in both the cost function and the norm of the gradient happen during the first few iterations. They basically reach their minimum values less than 20 iterations therefore the minimization procedure converges rather fast. In all cases, we run the minimization algorithm for 100 iterations, which should be sufficient for convergence.

Shown in Fig. 4 is the east-west vertical cross-section of the retrieved or analyzed 3D water vapor field (dashed lines) versus the 'true' moisture field (solid lines) at $y = 270$ km (along A-B line in Fig. 1). It can be seen that the analysis follows the 'truth' reasonably well. The moisture contours take an essentially vertical orientation at the location of dryline (about $x = 360$ km) below the 1.5 km level. This boundary separates the dry air from the high plateau to the west and the moist air originating from the Gulf of Mexico. The moisture ridges and troughs are found at the right locations and the extremum centers match the 'truth' well also.

This analysis using an isotropic recursive filter is actually much better than that obtained using an explicit isotropic Gaussian filter by LX05, when other configurations are the same. In the case of explicit filtering, the correlation has to be cut off at certain distance to keep the computational cost manageable. This action actually destroys the positive definiteness of the background error covariance although the effect is usually small. In the case of recursive filter, no cut-off radius is necessary so that the positive definite property is preserved. Much low computational cost is another advantage of the recursive filter. The time ratio of performing this analysis with recursive filter to with explicit filter is about 1/20. Obviously, such a performance difference is very significant for operational applications.

The analysis increment at the 5th terrain-following model level, or about 500 meters above the ground, is presented in Fig. 5a, together with the corresponding 'truth' increment ('truth' minus background, Fig. 5b). They show roughly similar patterns and extremum locations. The dryline can be recognized easily in the analysis. The overall correlation coefficient (CC) and the root-mean square error (RMSE) between the analysis increment and the 'truth' increment are presented in Table 1. The CC is as high as 0.78 and the RMSE is 0.43 g kg^{-1} , both indicating good analysis.

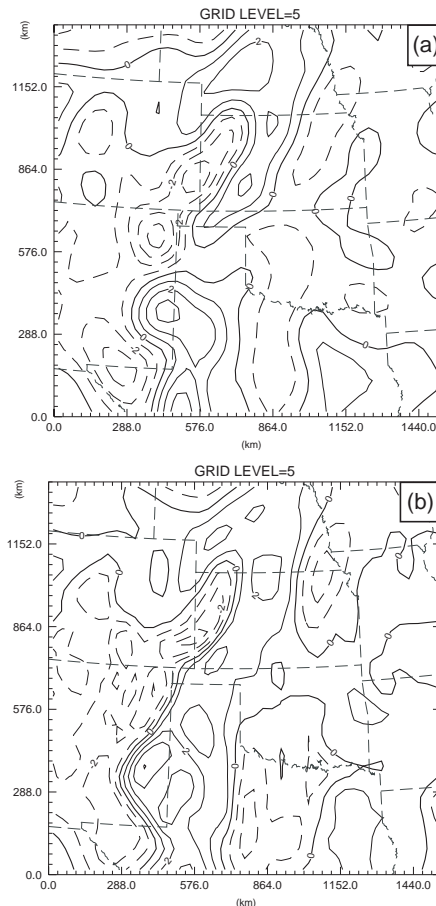


Fig. 5. (a) Analysis increment of q_v at the 5th grid level (ARPS model uses terrain-following coordinate. The mean height is about 500 meters above the surface). (b) 'Truth' minus background at the same level. The unit is g kg^{-1} and the contour interval is 1 g kg^{-1} .

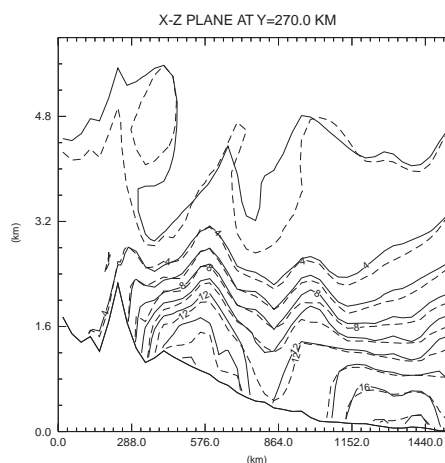


Fig. 6. As Fig. 4 but for experiment ANISO.

b. Analysis with an anisotropic background error correlation model

It has been realized for a long time that, of all the variables, the moisture particularly benefits from the provision of the anisotropy in the correlation functions used to construct the analysis increments. Fully anisotropic background error covariance is needed to obtain more accurate moisture analysis as well as to improve the quality of QPF. Another parallel experiment ANISO is to be performed to demonstrate how the anisotropic background error covariance improves the analysis. An anisotropic covariance replaces the isotropic one in this experiment and the chosen correlation scales are 5 grid intervals for L_r and 2.0 g kg^{-1} for L_f . The decision of the scales is given by the scale sensitivity tests described later. The background error shape is exactly true because the true moisture field is utilized in this idealized experiment. The weights of terms in cost function are the same to the Experiment ISO because observation data and background are not changed. Other parameters used for the filter are set identically as those in the ISO. The analysis vertical slice at $y = 270 \text{ km}$ is shown in Fig. 6. Obviously, there is a dramatic improvement in comparison to the analysis from ISO. The dryline structure is derived very well and contours almost coincide with the truth. Except that the basic pattern follows truth, the small-scale information is also shown clearly. For example, the $q_v = 14.0 \text{ g kg}^{-1}$ contour has a sharp fall down at $x = 620 \text{ km}$ and the derived moisture also shows this fine-scale structure. Further, the moisture ridge, at $x = 300 \text{ km}$ due to updraft, is recovered very well using anisotropic filter while it is missed using isotropic filter. In one word, the anisotropies in the moisture patterns do not diminish at smaller scales. The overall CC and RMSE for experiment ANISO are respectively 0.9256 and 0.2489 g kg^{-1} , presented in Table 1. It is believed that the good quality of the analysis contributes from the smoothing direction determined by ‘aspect tensor’.

c. Anisotropic analysis based on estimated background error field

With the elegant accomplishment of the retrieval of detailed dryline structures, experiment ANISO has distinctly verified that it is desirable to owe a more control over the form and degree of anisotropy than one based on randomly predefined coordinate choices. The reliable estimation of the degrees and orientations of anisotropy in the moisture background errors is crucial to the success of the analysis. Unfortunately, we never know the ‘truth’ or true background error. So far, the ensemble method can provide a reasonable flow-dependent background error covariance, but it takes too much computational time.

Hence, we seek another procedure to estimate the moisture field which is utilized to compute the flow-dependent background error correlation. The analysis increment from experiment ISO is considered as the estimate of the background error of moisture field, i.e., it is taken as f in Eq. (6) so as to provide an adaptive background error correlation. Hence, another parallel experiment is performed with same background and all the parameter settings as in the experiment ANISO, and it is called UB which means it updates the \mathbf{B} from isotropic to anisotropic. This method is performed in two steps iteratively. The background error covariance in the second step is a function of the analysis from the first step. The update of covariance supports the improvement of analysis. This method is feasible and easy to implement. The background error correlation is updated outside the minimization process so that it is not involved complicated nonlinear process.

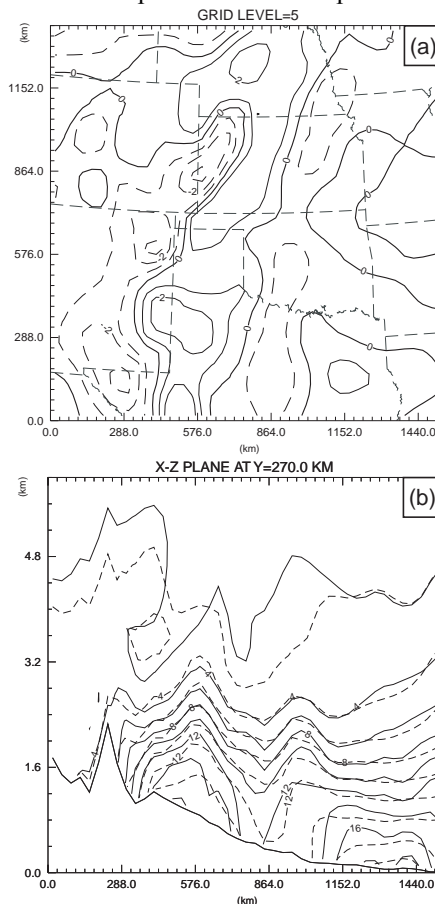


Fig. 7. (a) Analysis increment of q_v in unit g kg^{-1} at the 5th grid level from experiment UB with interval 1 g kg^{-1} , where dashed lines are for negative values and solid lines for positive values. (b) East-west vertical cross-section of q_v at $y = 270 \text{ km}$ with interval 2 g kg^{-1} . Solid lines are for ‘nature’ run and dashed lines for experiment UB.

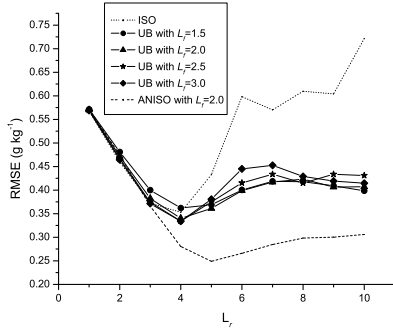


Fig. 8. The overall RMSE (g kg^{-1}) between retrieved 3D analysis increments and the 'true' increment ('truth' minus background), as a function of the decorrelation scale L_r (in units of analysis grid intervals). The dotted line is for experiment ISO, dashed line for experiment ANISO with $L_f = 2 \text{ g kg}^{-1}$ and solid lines for experiment UB with $L_f = 1.5, 2.0, 2.5, 3.0 \text{ g kg}^{-1}$, respectively.

Experiment	Observation errors	anisotropic Filter	CC	RMSE (g kg^{-1})
ISO	No	No	0.7844	0.4328
ANISO	No	Yes	0.9256	0.2489
UB	No	Yes	0.8388	0.3610
UB_err	5% sfc error 7% SWV error	Yes	0.7754	0.4494

Table 1. List of retrieval experiments. In this table, SWV denotes GPS slant-path water vapor data and 'sfc' denotes the surface moisture observation data. CC is the overall correlation coefficient and RMSE is the root-mean square error between the derived moisture increment and the 'true' moisture increment ('truth' minus background).

For OSSE, we can compute the 'true' background error covariance \mathbf{B} . And the \mathbf{B} matrixes for experiments ISO and UB, referred as \mathbf{B}_{ISO} and \mathbf{B}_{UB} respectively, can be calculated using Eq. (5) and (6). If the distance of two matrixes is defined as the norm of the corresponding component differences of the two matrixes, then the distance between \mathbf{B}_{ISO} and true \mathbf{B} and between \mathbf{B}_{UB} and true \mathbf{B} can be obtained easily according to our definition. Their ratio is about 2.5, i.e., the \mathbf{B}_{UB} is two and half times closer to the true \mathbf{B} than the \mathbf{B}_{ISO} . The analysis from this experiment UB is shown in Fig.7. The analysis increment at the 5th grid level (Fig. 7a) is more stretched along the dryline direction in comparison with the analysis from experiment ISO. The anisotropy is represented obviously by the contour $q_v = 4$ and 6 g kg^{-1} (Fig. 7b). The fine-scale ridge (at $x = 300 \text{ km}$) and troughs (at $x = 500 \text{ km}$ and 832 km) are displayed more

clearly than that with isotropic filter (experiment ISO) except that the main ridge and trough follows the 'truth'. These fine-scale structures maybe play a key role for the accurate QPF. The overall evaluation score again reveals the updated B method improves the analysis. CC increases from 0.7844 to 0.8388 and RMSE decreases from 0.4328 g kg^{-1} to 0.3610 g kg^{-1} .

6. Sensitivity tests

a. Sensitivity to decorrelation scale

The quality of analysis is closely related to the decorrelation scale defined in Eqs. (5) and (6), we therefore examine in this section how the analysis quality varies with the decorrelation scale, in terms of the CC and RMSE. In these sensitivity experiments, the weights for the different terms in the cost function take the same values as experiment ISO. In the isotropic case, only L_r is a free parameter. Taking advantage of our knowledge of the 'true' moisture, we can explore the parameter space of L_r in order to find a value that yields the best analysis. In Fig. 8, the dotted line shows the RMSEs as a function of L_r (in units of analysis grid intervals). We see that the optimal correlation scale length is equal to four grid intervals for this isotropic case. This is reasonable because the ground receiver spacing of the assumed network is equal to four grid intervals. This optimal decorrelation length matches the observation density and yields an overall correlation of up to 0.844 and the overall RMSE is as low as 0.353 g kg^{-1} .

Likewise, in the anisotropic case, there are two free parameters L_r and L_f , so we scan the parameter space of the correlation model in order to find the set of (L_r, L_f) that yields the best analysis. The solid lines in Fig. 8 are the RMSE as a function of L_r with different L_f values for experiment UB. We only test four values 1.5, 2.0, 2.5 and 3.0 because other values are not physically reasonable. The comparison of solid lines suggests the optimal correlation scale set is $L_r = 4$ grid intervals and $L_f = 3.0 \text{ g kg}^{-1}$. The differences between these four solid lines are tiny and $L_f = 2.0 \text{ g kg}^{-1}$ gives the overall better analysis than other three. For anisotropic filter, the optimal set of parameters also depends on the field that is analyzed except on the L_r . For realistic use, the choice of the scale should depend on the density and physical distribution of the observation network. Because it is rare to accidentally choose the optimal scales, we can only expect the scales near the optimal can be chosen with the knowledge of observation density. If the scale is chosen too small, the gap between two observation stations can not be covered so that the first guess can not be modified at some grid points far away from the observation stations. On the contrary, too large correlation scale essentially drives the analysis too smoothed. The reasonable scale, therefore, is around

four grid interval for this case. Three and five grid intervals are reasonable as the correlation scale. So our previous retrieval experiments select $L_r = 5$ grid intervals and $L_f = 2.0 \text{ g kg}^{-1}$.

The dashed line in Fig. 8 is the variation of RMSE for the most ideal experiment ANISO with L_r given $L_f = 2.0 \text{ g kg}^{-1}$. It is obvious that experiment ANISO always provides the best analysis with same background and parameter settings as those in experiments ISO and UB. The comparison between solid lines and dotted line in Fig. 8 also demonstrates that the utility of anisotropic filter always gives better analysis than that of isotropic filter, even more improvement when the L_r is larger than 4 grid intervals. It verifies the analysis from experiment UB is better than that from experiment ISO from another viewpoint. The RMSE considerably increase with the L_r , when L_r is larger than 4 for isotropic case while no significant worsening happens for anisotropic case, so it is proper to take larger L_r to avoid some gap for anisotropic case. The L_f controls the distance to which the innovation information spread together with the L_r for anisotropic case. Larger L_r allows two grids far away from each other to be correlated, but their correlation would be reduced significantly if their physical characteristics hold big difference, e.g., dry air from Plains region and moist air from Gulf of Mexico. That is the reason that the analysis does not considerably go worse with L_r for anisotropic cases represented by solid lines.

b. Sensitivity to observational errors

All afore-mentioned experiments use simulated GPS *SWV* and surface moisture data which include no observation errors. In practical use, however, the observations would not be error free, so it is crucial to test the analysis sensitivity to the observation errors. Experiment UB_err repeats the experiment UB but with observation errors in which normally distributed errors with 5% and 7% standard deviations are added to the simulated surface and *SWV* observations, respectively. The *SWV* errors are consistent with the estimate of Braun et al. (2001) for real data. The relative weights for *SWV* and surface observation terms are decreased to 80 and 400, respectively, because of the added observational errors. The analysis from this experiment also matches the 'truth' reasonably well (figure not shown). Hence, in the presence of realistic errors in the *SWV* and surface observations, our variational retrieval system with recursive filter is still powerful to produce good analysis, although the overall correlation coefficient of the increments decreases from 0.8388 to 0.7754 and the RMSE increases from 0.3610 g kg^{-1} to 0.4494 g kg^{-1} (Table 1). All major structures of the dryline are recovered well.

7. Conclusions

In our previous study (Liu and Xue 2005), an explicit spatial filter is applied to model both the background error covariances that can be flow dependent. In that case, both computational and memory storage costs are high even with moderate cut-off radii for the spatial correlation function. A computationally much more efficient algorithm based on the recursive filter is implemented and evaluated in this study, for the purpose of analyzing 3D water vapor fields from simulated GPS *SWV* observations. Surface moisture observations collected at the ground receiver sites are analyzed at the same time. This study represents the first time that a fully anisotropic recursive filter is used for modeling flow-dependent background errors in the context analyzing GPS observations. The main conclusions are listed as follows.

- 1) The isotropic recursive filter is found to produce better analysis than the corresponding isotropic explicit filter. Improved positive-definiteness property of the modeled background error covariance is believed to be the reason.
- 2) Anisotropic recursive filter, which is adaptive to the structure of the background error both in smoothing directions and decorrelation scales, produces much better analyses of specific humidity than the isotropic one, especially in fine-scale moisture structures.
- 3) In the absence of good knowledge about the background error, an iterative procedure for its estimation is proposed, in which an isotropic analysis is performed first. The difference between this tentative analysis and the background is used to define the error field needed by the background error covariance model. This estimated error field is then used in the second anisotropic analysis step. Improved analysis, compared to the isotropic analysis, is obtained through this procedure.
- 4) Experiments on the sensitivities of the analysis to the error de-correlation scales are performed. It is found that the isotropic analysis is more sensitive to the decorrelation scale L_r and the range of L_r within which good analysis is obtained is narrow. The analysis is much less sensitive to L_r , however, when the error-field dependent component of the background error is introduced. For the test case examined, the optimal geometric length scale L_r is found to be close to the mean distance between the GPS ground receiver stations.
- 5) The analysis procedure is found to be robust and not very sensitive to the presence of observational errors of typical magnitudes in the GPS *SWV* data and in the surface moisture observations.
- 6) Compared to the explicit filters examined in Liu and Xue (2005), the biggest advantage for using

recursive filters is the computational efficiency. The computational cost of a recursive filter is about one twentieth that of the corresponding explicit filter even when moderate cut-off radii are used with the latter. The quality of analyses are in general comparable, with the analysis obtained with recursive filter being somewhat better in some cases, due to, we believe, the positive definiteness of the background error covariance thus modeled.

In the near future, we will use the analyzed moisture field to initialize a mesoscale model, such as the ARPS, and examine the impact of assimilating GPS *SWV* data on short-range precipitation forecasts. The assimilation and examination of the impact of real GPS *SWV* data collected during the IHOP_2002 field experiment are also planned.

Acknowledgement

This work was mainly supported by NSF grant ATM-0129892. Xue was also supported by NSF grants ATM-0331756, ATM-0331594, EEC-0313747, a DOT-FAA grant via DOC-NOAA NA17RJ1227, and by "Outstanding Overseas Scholars" awards from Chinese Natural Science Foundation (No. 40028504) and from Chinese Academy of Sciences (No. 2004-2-7). Drs. Keith Brewster, Jidong Gao, and William Martin are thanked for helpful discussions.

References

- Braun, J., C. Rocken, and R. Ware, 2001: Validation of line-of-sight water vapor measurements with GPS. *Radio Sci.*, **36**, 459-472.
- Courtier, P., J.-N. Thepaut, and A. Hollingsworth, 1994: A strategy for operational implementation of 4D-Var, using an incremental approach. *Quart. J. Roy. Meteor. Soc.*, **120**, 1367-1387.
- Cucurull, L., F. Vandenberghe, D. Barker, E. Vilaclara, and A. Rius, 2004: Three-dimensional variational data assimilation of ground-based GPS ZTD and meteorological observations during the 14 December 2001 storm event over the western mediterranean sea. *Monthly Weather Review*, **132**, 749-763.
- De Pondeca, M. S. F. V. and X. Zou, 2001a: Moisture retrievals from simulated zenith delay "observations" and their impact on short-range precipitation forecasts. *Tellus*, **53**, 192.
- , 2001b: A Case Study of the Variational Assimilation of GPS Zenith Delay Observations into a Mesoscale Model. *Journal of Applied Meteorology*, **40**, 1559-1576.
- Falvey, M. and J. Beavan, 2002: The Impact of GPS Precipitable Water Assimilation on Mesoscale Model Retrievals of Orographic Rainfall during SALPEX'96. *Monthly Weather Review*, **130**, 2874-2888.
- Guo, Y.-R., Y.-H. Kuo, J. Dudhia, D. Parsons, and C. Rocken, 2000: Four-dimensional variational data assimilation of heterogeneous mesoscale observations for a strong convective case. *Mon. Wea. Rev.*, **128**, 619-643.
- Ha, S.-Y., Y.-H. Kuo, Y.-R. Guo, and G.-H. Lim, 2003: Variational Assimilation of Slant-Path Wet Delay Measurements from a Hypothetical Ground-Based GPS Network. Part I: Comparison with Precipitable Water Assimilation. *Monthly Weather Review*, **131**, 2635-2655.
- Hayden, C. M. and R. J. Purser, 1995: Recursive filter objective analysis of meteorological fields: applications to NESDIS operational processing. *J. Appl. Meteor.*, **34**, 3-15.
- Huang, X.-Y., 2000: Variational Analysis Using Spatial Filters. *Monthly Weather Review*, **128**, 2588-2600.
- Kuo, Y.-H., Y.-R. Guo, and E. R. Westwater, 1993: Assimilation of precipitable water measurements into a mesoscale numerical model. *Mon. Wea. Rev.*, **121**, 1215-1238.
- Kuo, Y.-H., X. Zou, and Y. R. Guo, 1996: Variational assimilation of precipitable water using a nonhydrostatic mesoscale adjoint model. Part I: Moisture retrieval and sensitivity experiments. *Mon. Wea. Rev.*, **124**, 122-147.
- Liu, H. and M. Xue, 2005: Retrieval of moisture from slant-path water vapor observations of a hypothetical GPS network using a three-dimensional variational scheme with anisotropic background error. *Mon. Wea. Rev.*, In review.
- MacDonald, A. E., Y. Xie, and R. H. Ware, 2002: Diagnosis of Three-Dimensional Water Vapor Using a GPS Network. *Mon. Wea. Rev.*, **130**, 386-397.
- Purser, R. J., W.-S. Wu, D. F. Parrish, and N. M. Roberts, 2003a: Numerical aspects of the application of recursive filters to variational statistical analysis. Part I: Spatially homogeneous and isotropic Gaussian covariances. *Monthly Weather Review*, **131**, 1524-1535.
- , 2003b: Numerical aspects of the application of recursive filters to variational statistical analysis. Part II: Spatially inhomogeneous and anisotropic general covariances. *Monthly Weather Review*, **131**, 1536-1548.
- Rocken, C., R. H. Ware, T. v. Hove, F. Solheim, C. Alber, J. Johnson, M. Bevis, and S. Businger, 1993: Sensing atmospheric water vapor with global positioning system. *Geophys. Res. Lett.*, **20**, 2631-2634.
- Ware, R., C. Alber, C. Rocken, and F. Solheim, 1997: Sensing integrated water vapor along GPS ray paths. *Geophys. Res. Lett.*, **24**, 417-420.

- Weckwerth, T. M., D. B. Parsons, S. E. Koch, J. A. Moore, M. A. LeMone, B. B. Demoz, C. Flamant, B. Geerts, J. Wang, and W. F. Feltz, 2004: An overview of the International H2O Project (IHOP_2002) and some preliminary highlights. *Bulletin of the American Meteorological Society*, **85**, 253-277.
- Xue, M., K. K. Droegemeier, and V. Wong, 2000: The Advanced Regional Prediction System (ARPS) - A multiscale nonhydrostatic atmospheric simulation and prediction tool. Part I: Model dynamics and verification. *Meteor. Atmos. Physics*, **75**, 161-193.
- Xue, M., D.-H. Wang, J.-D. Gao, K. Brewster, and K. K. Droegemeier, 2003: The Advanced Regional Prediction System (ARPS), storm-scale numerical weather prediction and data assimilation. *Meteor. Atmos. Physics*, **82**, 139-170.
- Xue, M., K. Brewster, D. Weber, K. W. Thomas, F. Kong, and E. Kemp, 2002: Realtime storm-scale forecast support for IHOP 2002 at CAPS. *Preprint, 15th Conf. Num. Wea. Pred. and 19th Conf. Wea. Anal. Forecasting*, San Antonio, TX, Amer. Meteor. Soc., 124-126.
- Xue, M., K. K. Droegemeier, V. Wong, A. Shapiro, K. Brewster, F. Carr, D. Weber, Y. Liu, and D.-H. Wang, 2001: The Advanced Regional Prediction System (ARPS) - A multiscale nonhydrostatic atmospheric simulation and prediction tool. Part II: Model physics and applications. *Meteor. Atmos. Phys.*, **76**, 143-165.